The 11th Canadian Conference on Earthquake Engineering
Canadian Association for Earthquake Engineering

SEISMIC RESISTANCE OF CIRCULAR GLASS FIBER REINFORCED POLYMER CONFINED CONCRETE COLUMNS

Arsalan Tavassoli
M.A.Sc. Candidate, University of Toronto, Canada
Arsalan.tavassoli@mail.utoronto.ca

Shamim A. Sheikh
Professor, University of Toronto, Canada
sheikh@ecf.utoronto.ca

ABSTRACT: GFRP is slowly gaining acceptability as a replacement of steel to address the issue of steel corrosion in concrete structures. To evaluate the feasibility of using GFRP spirals as internal reinforcement in columns, an extensive research program is underway at the University of Toronto. Sixteen 356 mm diameter concrete columns were tested under simulated earthquake forces, which included constant axial load and cyclic lateral displacement excursions. Each column contained six longitudinal steel bars. Lateral steel consisted of spirals in eight columns while the other eight columns had lateral GFRP spirals. This paper presents responses of selected specimens in the form of moment vs. curvature response, shear vs. deflection behaviour, and discusses ductility parameters related to curvature, displacement, and energy dissipation to evaluate the performance of columns. Columns reinforced with longitudinal steel and lateral GFRP spirals demonstrated excellent post elastic stable response accompanying large shear and moment capacities. Strength and ductility results of these specimens were similar to those of the fully steel reinforced columns.

1. Introduction

Recent estimates indicate that the annual cost of corrosion from all sectors worldwide in 2010 was about USD 2.2 trillion, which represents about 3% of the world's GDP of $73.33 trillion (Hays, 2010). About 16.4% of the total corrosion cost is from the infrastructure sector. Typically, corrosion happens in bridge decks, beams and columns. This has led to a $13.6 billion annual direct corrosion cost for highway bridges in the United States (NACE, 2013). In concrete columns, steel spirals are the first element to corrode since the concrete cover protecting these bars is typically not adequate to protect steel. As the steel continues to corrode, the buildup of rusts puts pressure on the surrounding concrete, causing cracking around the steel. Eventually, the concrete cover spalls off due to the expansion (See Fig. 1).

An important feature of fiber reinforced polymer composites (FRP) is their high corrosion resistance property. This characteristic of these non-metallic bars makes them suitable for use in structures subjected to corrosive environmental exposures. FRP as internal reinforcement has the potential to improve durability of concrete structures such as parking garages, multistory buildings, industrial structures, and bridges significantly.

Glass fiber reinforced polymer (GFRP) bars in member subjected to mostly flexure have been an active research area over the last several years but there is only very limited work done on columns. GFRP spirals/ties in columns will not corrode and prevent deterioration of the cover concrete. Although this new technology is gaining popularity with designers, its use is still minimal due to a lack of experimental data, design procedures and guidelines.

Fig. 1 – Corrosion of spirals in columns

2. Experimental Program

Sixteen circular concrete columns, 356 mm in diameter and 1470 mm long were constructed and tested at the Structures Laboratories at the University of Toronto. Each column had 6-25M longitudinal steel bars. Group 1 had eight columns that were reinforced with steel spirals (Liu, 2013), while group 2 consisted of eight columns that were reinforced with GFRP spirals. All sixteen columns were cast integrally with a stub approximately measuring 484 × 700 × 800 mm and represented a discontinuity like a beam column joint or a footing adjacent to the section of maximum moment. Refer to Fig. 2 for a schematic of the specimen and column cross section.

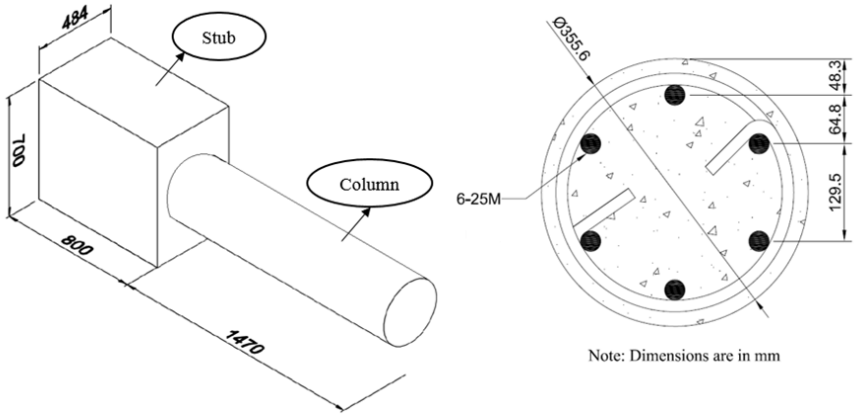

Fig. 2 – Specimen and cross-section of column

Due to the space limitation, the authors have discussed results from four columns of group 1 and two of group 2 in this paper to highlight the effects of different variables including the type of lateral reinforcement, steel or GFRP. Table 1 provides general information regarding these six specimens and highlights two sets of columns; each includes one GFRP confined column and two steel confined columns. All parameters among the three specimens in each set were similar, except the spiral spacing or spiral ratio as noted in Table 1.

Table 2 and Table 3 provide information regarding the material properties of steel and GFRP used in the six specimens.

Table 1 – Specimen Details

Specimen (Group number)	Concrete Strength f'c (MPa)	Axial Load $/P_0$	Lateral Reinforcement	Lateral Reinforcement Size (mm) @ spacing (mm)	Lateral Reinforcement Ratio (%)
P27-NF-1 (1)	40	0.27	Steel	US #3 @ 150	0.60
P27-NF-2 (1)	40	0.27	Steel	US #3 @ 100	0.90
P28-LS-12-160 (2)	40	0.28	GFRP	12 @ 160	0.94
P56-NF-11 (1)	40	0.56	Steel	10M @ 100	1.22
P56-NF-12 (1)	40	0.56	Steel	10M @ 75	1.63
P55-LS-12-90 (2)	41	0.55	GFRP	12 @ 90	1.67

Table 2 – Mechanical properties of GFRP spirals

Rebar type	Bar application (Group number)	Nominal diameter (mm)	Actual diameter (mm)	Modulus of elasticity (MPa)	Ultimate stress (MPa)	Ultimate strain
GFRP	Spiral (2)	12	12.25	58500	1050	0.0179

Table 3 – Mechanical properties of steel bars

Rebar type	Bar Application (Group number)	Area, A_S (mm^2)	Yield strength, f_y (MPa)	Yield strain, ε_y	Elastic modulus, E_s (MPa)	Start of Strain hardening, ε_{sh}	Ultimate strength, f_u (MPa)	Strain at ultimate strength, ε_u
25M	Longitudinal (1)	500	490	0.0024	201136	0.0250	641	0.196
25M	Longitudinal (2)	500	463	0.0025	194000	0.0086	645	0.140
10M	Spiral (1)	100	450	0.0024	191431	0.0213	583	0.212
US#3	Spiral (1)	71.3	496	0.0025	198580	0.0283	605	0.171

Fig 3. shows all group 2 specimens before testing. One layer of carbon fiber reinforced polymer sheet was wrapped around the top portion of the columns to provide additional confinement to that area and to ensure that failure occurs within the instrumented test region close to the column-stub interface.

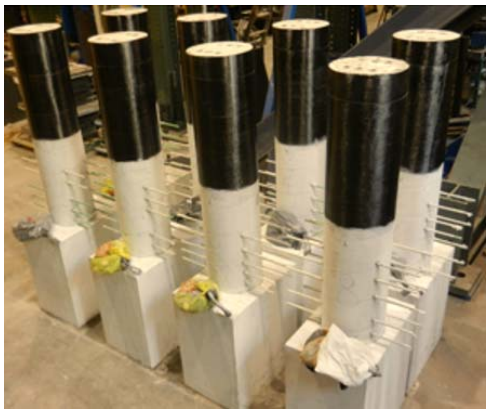

Fig. 3 – Specimens before test

We tested the specimens horizontally and subjected them to simultaneous constant axial load and cyclic quasi-static lateral displacement excursions in the Column Testing Frame (CTF) shown in Fig. 4. Fig. 5. displays the lateral displacement protocol used for testing of columns. The peak displacement of the first

cycle was 0.75Δy, followed by two cycles of Δy, 2Δy, 3Δy, and so on. The nominal yield deflection, Δy, of approximately 8.4 mm was used in group 1 specimens, while approximately 4.2 mm was used in group 2 specimens. The difference between the two values is because the actual yield deflection was used in group 1 specimens, while the theoretical yield deflection was used in group 2 specimens. The theoretical Δy is the deflection corresponding to the maximum load on the line joining origin to the point at 65% of the maximum load on the shear load vs lateral deflection curve. An axial load of 1281 kN ($0.27P_0$) or 2657 kN ($0.56P_0$) was applied to group 1 columns and similar axial load of 1243 kN ($0.28P_0$) or 2450 kN ($0.55P_0$) was applied to group 2 columns. P_0 is the nominal axial load capacity of column. The line of action of the axial load stayed constant throughout the duration of the test. The vertical MTS actuator in CTF applied the lateral load at the stub (approximately 150 mm away from the stub-column interface), so that the most critically loaded region of the column was the column-stub interface and subjected to combined flexure, shear and axial load.

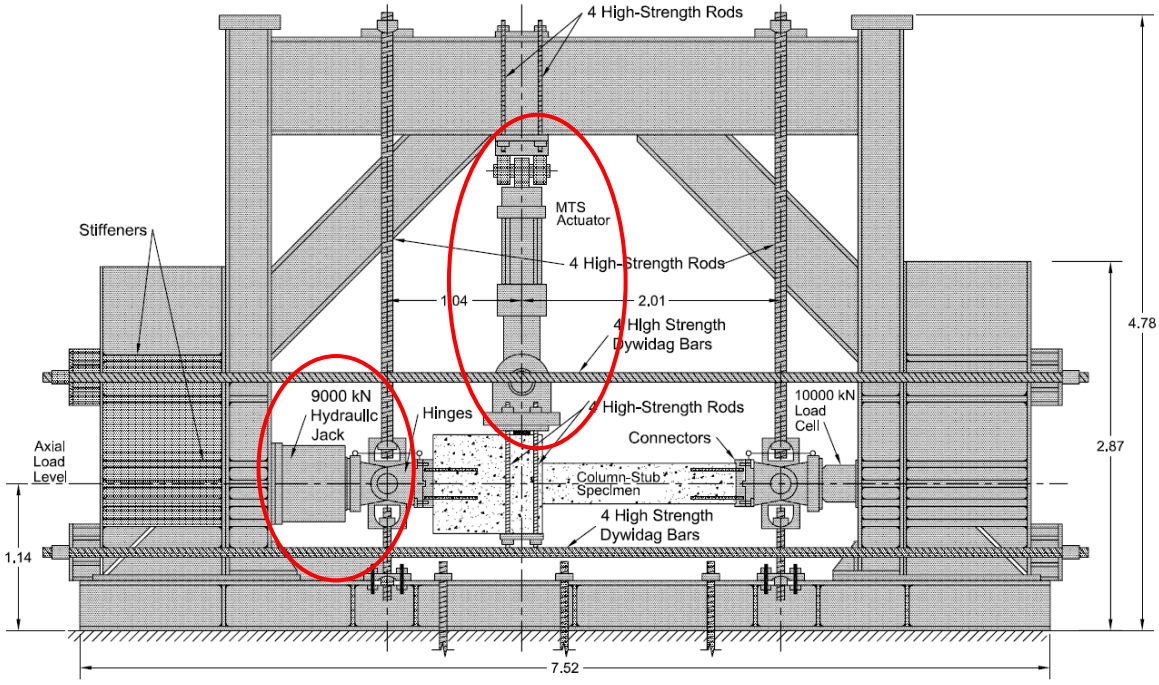

Fig. 4 – Column Testing Frame (CTF)

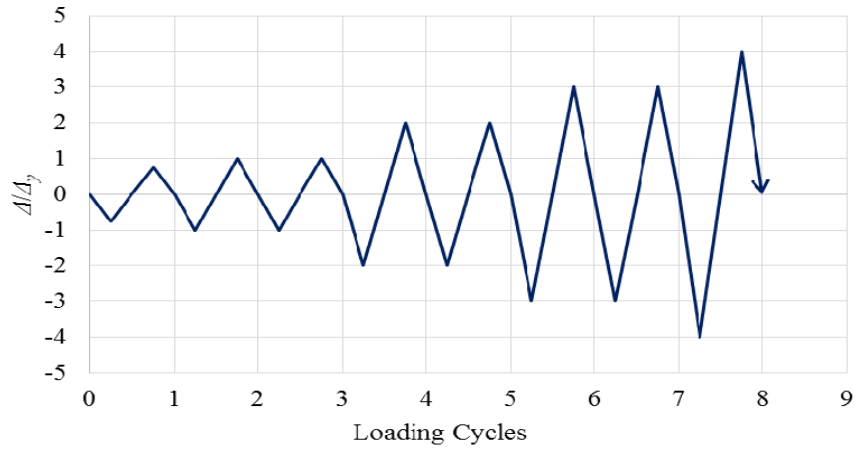

Fig. 5 – Lateral displacement excursions

Fig. 6 presents a schematic drawing of a specimen in the horizontal test set up and it‘s relation to a portion of a column standing vertically in a real life application. The actual shear span of column is 1840 mm, which extends from the column-stub interface to center of the right steel hinge. The shear span to depth ratio of the column was thus 5.17, where the outside column diameter is the depth of the column.

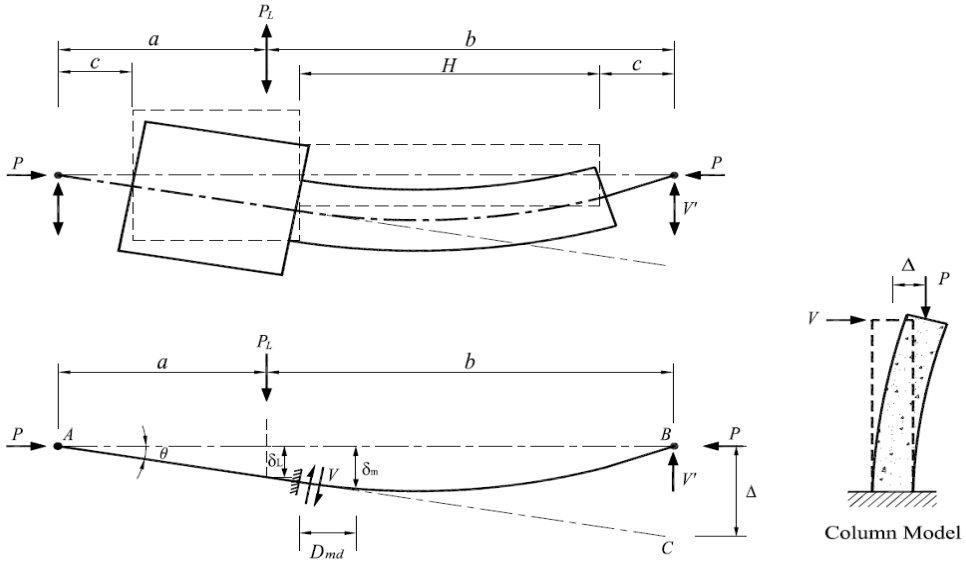

Fig. 6 – Schematic drawing of specimen under test

3. Experimental Results

In group 1 specimens, first visible sign of distress was the propagation of tiny flexural cracks that appeared on the top and bottom surfaces of the columns during the first cycle of lateral load. Additional cracks emerged and existing cracks widened gradually as the lateral deflection increased in the following two cycles. Concrete cover spalling initiated after the third lateral cycle and it spalled off around the two peak points of the fourth lateral excursion cycle with a peak deflection of $2\Delta_y$. After three lateral cycles, longitudinal cracks also occurred on the surface of columns along the longitudinal bars in the most compressed zone, which indicated the tendency of buckling of the longitudinal bars. In subsequent cycles, the buckling bars, together with the expanding concrete core, pushed spirals outward. Finally, the spirals fractured in an explosive manner, resulting in the failure of columns with the severe buckling of longitudinal bars and the crushing of the concrete core within the plastic-hinge region.

Bayrak and Sheikh (2001) observed the concept of premature buckling in longitudinal steel bars in square and rectangular columns. In order to prevent premature buckling of these bars under cyclic loading a spiral pitch to bar diameter ratio of less than six was deemed necessary. This means that premature buckling of a 25M bar occurs if the spiral pitch is greater than 150 mm, which matches with the experimental results from these tests.

In group 2 specimens, concrete cracks and spalling occurred at levels of displacement excursion similar to those observed for group 1 specimens. Longitudinal steel bars buckled prior to rupture of GFRP spirals in columns with spiral pitch of 160 mm. In the specimen with spiral pitch of 90 mm, longitudinal bars showed some sign of buckling during a cycle prior to rupture of spirals.

The confinement provided to the core concrete and the support provided to the longitudinal bars vanished as soon as the GFRP spiral ruptured. A combination of buckling of the longitudinal bars in compression accompanied by the crushing of the concrete core in the most damaged zone led to termination of the test.

Fig. 7 shows the most damaged regions after failure of the six specimens discussed here. The shifting-away of the most damaged section from the maximum moment section at the column-stub interface is due to the additional confining effect by the heavily reinforced concrete stub.

Fig. 7 – Columns after testing (in clockwise direction, starting from top left): P27-NF-1, P27-NF-2, P28-LS-12-160, P56-NF-11, P56-NF-12, and P55-LS-12-90

The first set in Table 1 includes three comparable specimens under approximately 1250 kN of axial load. Fig. 8 shows Shear (V) vs. tip deflection (Δ) and moment (M) vs. curvature (Φ) hysteresis relations for these three columns. The moment-curvature responses shown are for the most damaged sections of the columns.

Following points provide explanation for the graphs used in Fig. 8:

- Red horizontal line on the M - Φ response indicates the nominal unconfined moment capacity (M_n) of the section.
- Slopped red line on the V - Δ represents the nominal shear capacity V_n with a decreasing slope caused by secondary P - Δ effects.
- Red dots indicate the initiation of small cracks up to 0.3 mm in width.
- Light blue and dark blue dots represent the start of concrete cover spalling at bottom and top surfaces, respectively.
- Purple dots indicate the yielding of steel spiral
- Green dots signify the rupture of spiral
- Orange dots indicate buckling of the longitudinal bar(s)

The second set in Table 1 contains three specimens under approximately 2550 kN of axial load. Fig. 9 and Fig. 10 show V – Δ and M – Φ hysteresis relations and envelope curves for these three columns, respectively.

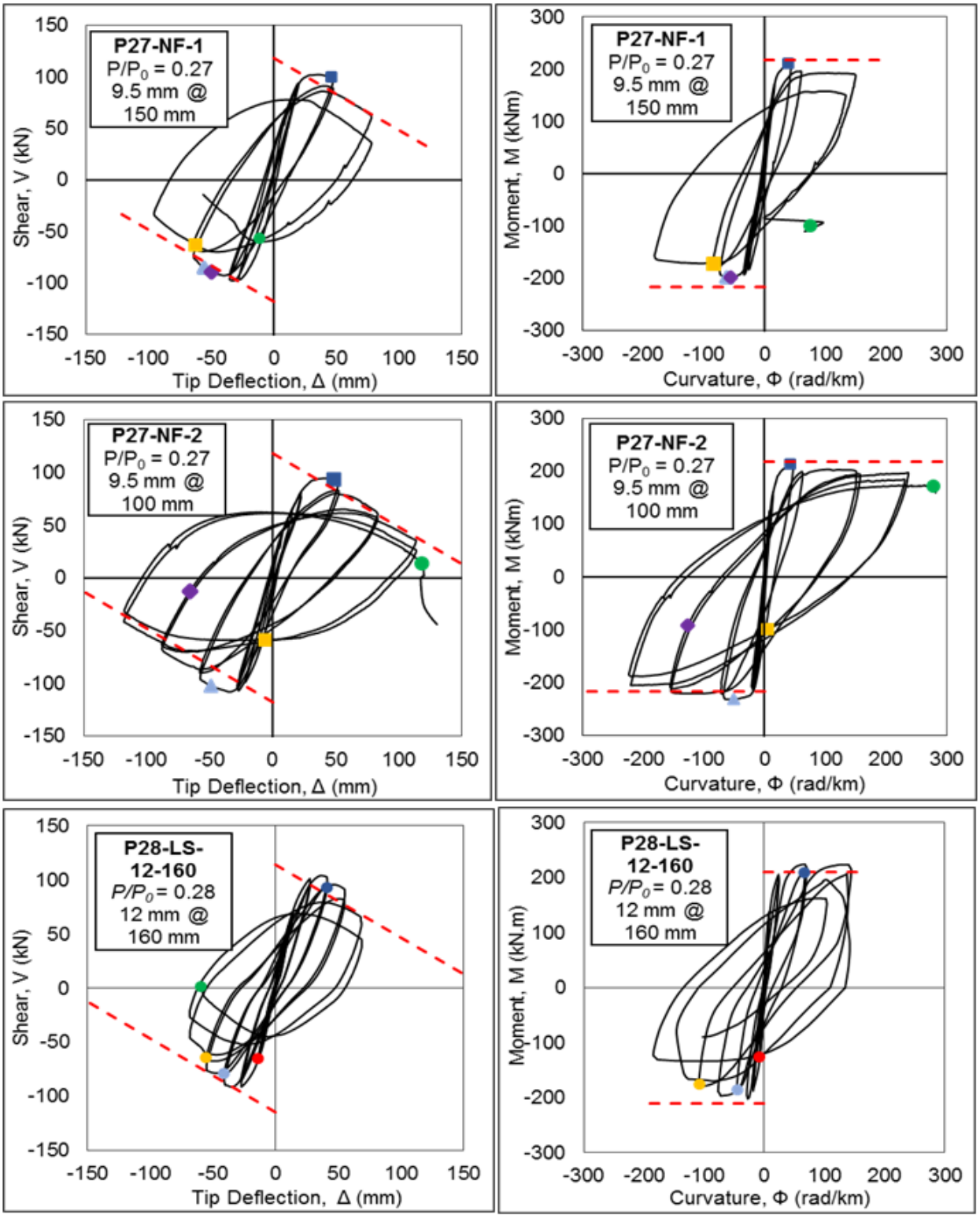

Fig. 8 – Shear vs. deflection and moment vs. curvature hysteresis (P/P_0 ~ 0.28)

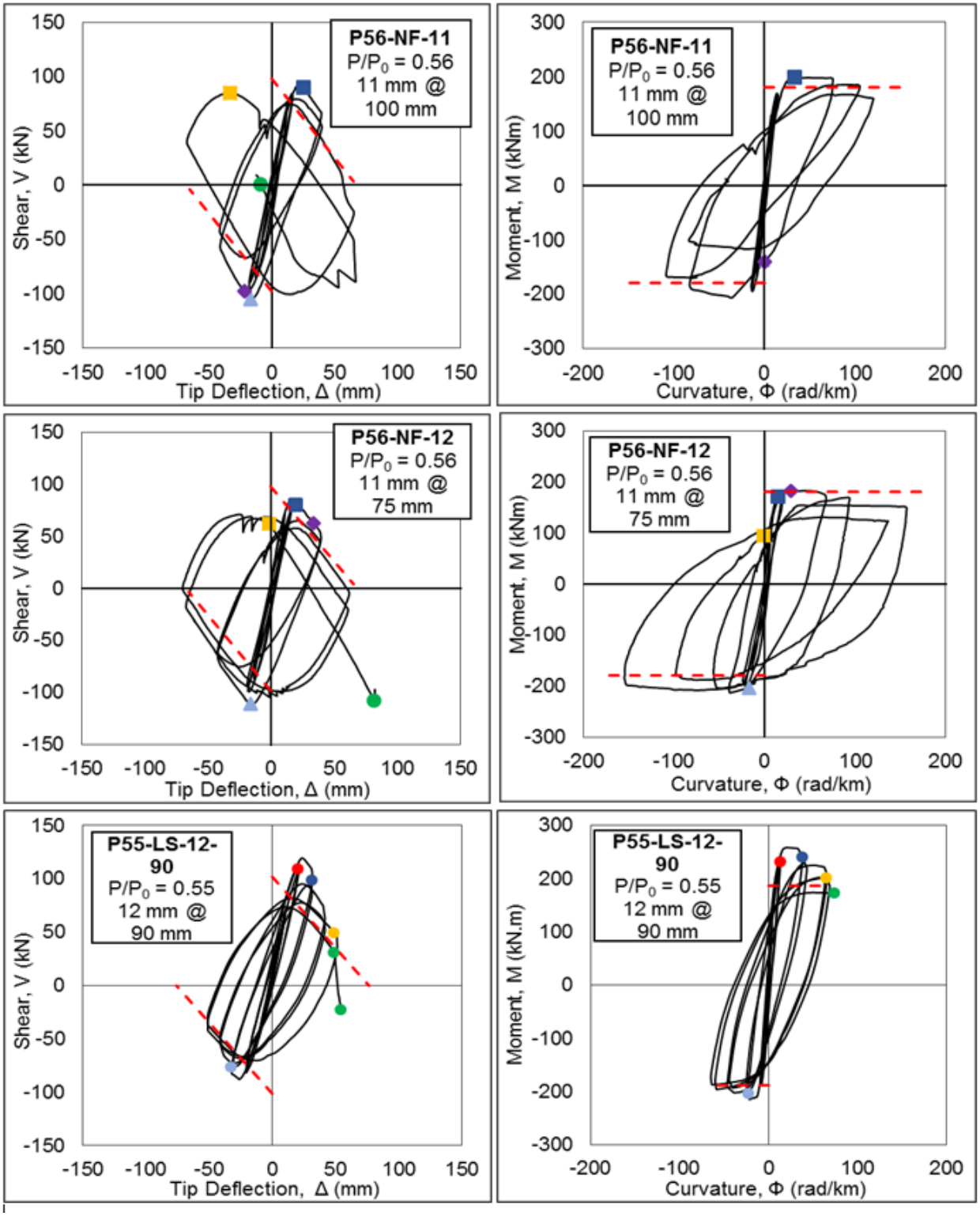

Fig. 9 – Shear vs. deflection and moment vs. curvature hysteresis (P/P_0 ~ 0.55)

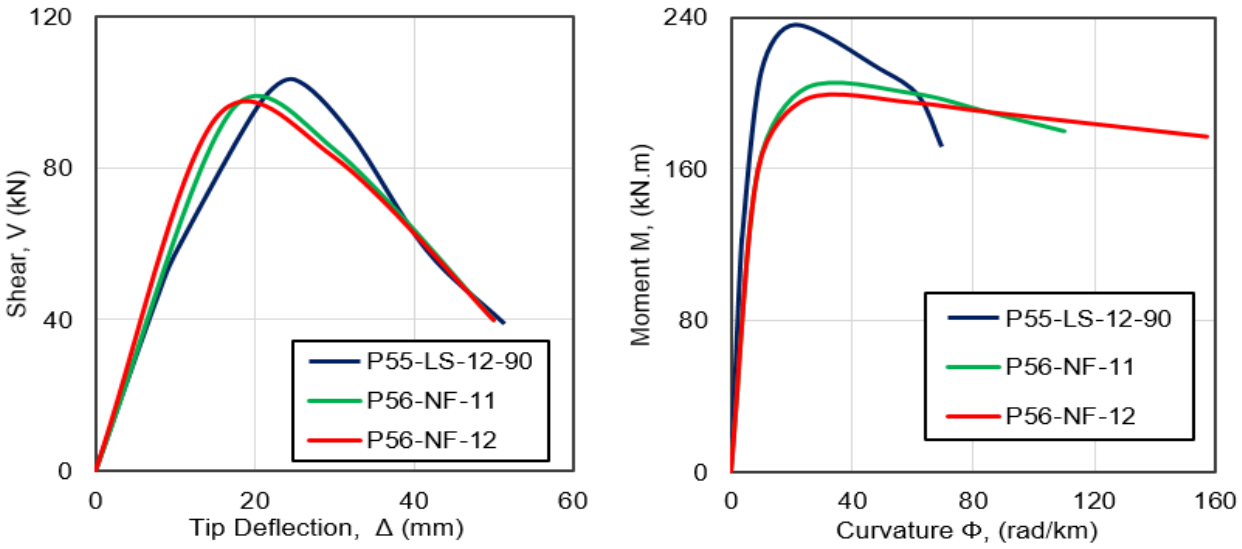

Fig. 10 – Shear vs. deflection and moment vs. curvature envelope curves (P/P_0 ~ 0.55)

Table 4 shows displacement ductility factor (μ_Δ), curvature ductility factor (μ_Φ), drift ratio (δ), maximum shear (V_{max}), maximum moment (M_{max}), and nominal moment capacity (M_n) for each specimen.

Table 4 – Summary of test results

Specimen (Group number)	μ_Φ	μ_Δ	δ (%)	V_{max} (kN)	M_{max} (kN.m)	M_n	M_{MAX} / M_N
P27-NF-1 (1)	12.6	3.4	3.2	100	204	217	0.94
P27-NF-2 (1)	19.8	3.8	3.5	101	220	217	1.01
P28-LS-12-160 (2)	11.1	3.1	3.1	98	210	210	1.00
P56-NF-11 (1)	12.8	3.3	2.2	95	203	180	1.13
P56-NF-12 (1)	18.2	3.7	2.1	93	197	180	1.09
P55-LS-12-90 (2)	12.7	2.9	2.2	104	234	187	1.25

4. Discussion

All columns reached similar maximum shear values since this parameter is mostly a function of column size, concrete strength, and longitudinal bars. Column confinement and level of axial load do not significantly influence the maximum shear when failure is caused by flexure.

Group 1 specimens are more ductile when the spiral pitch is smaller relative to that in specimens from group 2. However, specimens confined with GFRP or steel provide comparable levels of ductility when spiral spacing is similar. As shown in Table 4, displacement and curvature ductility factors along with lateral drift ratio of P27-NF-1 vs. P28-LS-12-160 and P56-NF-11 vs. P55-LS-12-90 are all within 10% since the spiral pitch in the compared specimens was similar.

Use of FRP transverse reinforcement would improve corrosion resistance of a column due to non-corrosive properties of spiral GFRP and by adding an extra 15 mm cover to longitudinal steel. The moment capacity of group 2 columns is approximately 15% higher than that of group 1 columns as observed in the M-Φ envelope curves shown in Fig. 10. This increase diminishes as spiral spacing increases and strength of columns confined with GFRP or steel becomes almost equal. The ratio of maximum moment to the unconfined moment capacity is close to one for specimens tested under lower axial load levels. This ratio varied from 1.1 to 1.25 for columns tested under higher axial load levels.

The experimental lateral drift ratio for specimen P28-LS-12-160 was 3.1%. According to CSA-S806-12, this column could be part of a moderately ductile moment-resisting frame. Meanwhile, the lateral reinforcement ratio provided in this column was only 0.94%, which is almost half of the required amount recommended by the code to reach 2.5% lateral drift ratio. This shows that the requirements for spiral ratio of the CSA-S806-12 code are quite conservative. Furthermore, it is important to note that the ductility parameters increase considerably as the spiral spacing decreases; and the columns are less ductile under higher axial loads.

Overall the results show that GFRP-confined columns can be used in seismic force resisting systems given enough care is taken in detailing and design process.

5. Concluding Remarks

Application of GFRP spirals mitigates the corrosion of steel reinforcement in concrete and hence improves durability of structures. Results from this study show that the overall strength and ductility of columns confined with GFRP were similar to those confined with steel. Thus, GFRP spirals can be efficient as primary lateral reinforcement for shear and confinement in concrete columns designed for seismic resistance even when they are subjected to large axial loads.

6. Acknowledgement

IC-IMPACTS, an NSERC network of Centres of Excellence, provided the financial support for this work. The first author also acknowledges the NSERC scholarship and Alexander Graham Bell Canada Graduate Scholarship. The experimental work reported here was carried out in the Structures Laboratories of the University of Toronto.

7. References

Bayrak, O., and Sheikh, S.A., “Plastic Hinge Analysis”, Journal of Structural Engineering, ASCE, 127(9), 2001, pp. 1092-1100.

Canadian Standards Association, (2012). “Design and Construction of Building Structures with Fibre-Reinforced Polymers.” Standards Council of Canada, Mar. 2012, Mississauga, ON, Canada.

Hays, G. F., (2010) NACE-International, The corrosion society.
http://events.nace.org/euro/corrodia/Fall_2010/wco.asp (Jan. 09, 2015)

NACE-International (2013), Corrosion Central, Industries and Technologies, Highways and Bridges
http://www.nace.org/Corrosion-Central/Industries/Highways-and-Bridges/ (Mar. 30, 2015)

Liu, J., (2013). “Seismic Behavior of Reinforced Concrete Columns.” Ph.D. Thesis, University of Toronto, Toronto, ON, 327 pp.